Multiple Gas Detection by Cavity-Enhanced Raman Spectroscopy with Sub-ppm Sensitivity

Qing-ying Yang, Yan Tan,* Zi-han Qu, Yu Sun, An-wen Liu, and Shui-ming Hu*

Read Online

ACCESS | 📊 Metrics & More | 📖 Article Recommendations | 🔘 Supporting Information

ABSTRACT: Accurate and sensitive detection of multicomponent trace gases below the parts-per-million (ppm) level is needed in a variety of medical, industrial, and environmental applications. Raman spectroscopy can identify multiple molecules in the sample simultaneously and has excellent potential for fast diagnosis of various samples, but applications are often limited by its sensitivity. In this contribution, we report the development of a cavity-enhanced Raman spectroscopy instrument using a narrow-line width 532 nm laser locked with a high-finesse cavity through a Pound-Drever-Hall locking servo, which allows continuous measurement in a broad spectral range. An intracavity laser power of up to 1 kW was achieved with an incident laser power of about 240 mW, resulting in a significant enhancement of the Raman signal in the range of 200−5000 cm^{-1} and a sub-ppm sensitivity for various molecules. The technique is applied in the detection of different samples, including ambient air, natural gas, and reference gas of sulfur hexafluoride, demonstrating its capability for the quantitative measurement of various trace components.
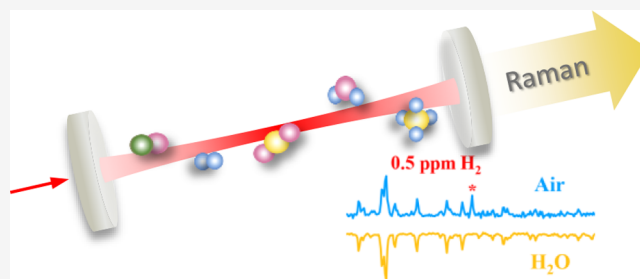
INTRODUCTION

Trace gas detection has extensive applications such as breath analysis,[1] industrial control,[2,3] environmental science,[4,5] and atmospheric and astronomic chemistry.[6,7] Usually, the detection limits of the gas contents in a given sample are required to reach the level of ppmv (μmol/mol) or even ppbv (10^{-3} μmol/mol). Trace gas detection based on laser spectroscopy can achieve high sensitivity, fast response, real-time, and in situ monitoring without consuming gas samples.[8] Direct absorption spectroscopy has good quantitative measurement ability,[9,10] and the detection limit can be improved to the parts per billion volume (ppbv) or even lower level by increasing the effective absorption optical path.[11,12] However, it cannot detect homonuclear diatomic molecules without electric dipole transitions such as N_2 and H_2. In addition, lasers of different wavelengths are required to detect different gases, respectively, which is not suitable for detecting mixed gas with multiple components.

Raman scattering signals are fingerprints of molecules, and the intensity of the Raman signal (I_{Raman}) could be written as[13]

$$I_{Raman} = \varepsilon I_{pump} l_{eff} \sigma_{Raman} N \tag{1}$$

where ε is the detection efficiency, I_{pump} is the intensity of the pump laser, N is the molecular number density, l_{eff} is the effective interaction length, and σ_{Raman} is the Raman scattering cross-section of the molecule. Raman spectroscopy can detect almost all molecules except monatomic molecules, and it can use a single laser source to achieve rapid measurement of

multiple gases at the same time.[14] However, due to the small Raman scattering cross sections of most gas molecules, the measurement sensitivity can hardly reach the level below 1 ppmv, which limits the application of Raman spectroscopy in trace gas detection.[15−19]

Since the molecular Raman scattering signal is proportional to the product of the excitation light intensity and the laser path length, using a resonant optical cavity to increase the effective light intensity can significantly improve the detection sensitivity of Raman spectroscopy, that is, cavity-enhanced Raman spectroscopy (CERS). CERS can achieve multigas real-time measurements with high selectivity, high sensitivity, low cost, and miniaturization, which result in wide applications in various scientific and industrial fields.[2,20,21] There has been much recent progress in CERS with improved detection limits. Taylor et al.[22] stabilized a 1 W laser in an optical cavity, obtained an intracavity laser power of 50 W, and achieved a detection limit of H_2 at the 10 ppm level. Hippler et al.[17] reported a CERS device based on an optical feedback diode laser. Using a diode laser with a power of 10 mW, they increased the intracavity laser power by 3 orders of magnitude
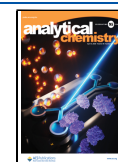
and recorded Raman spectra of air, CH_4, H_2, and benzene at the parts per million level. Wang et al.[23] used a three-mirror V-shaped optical cavity to boost the intracavity laser power from 105 mW to 222 W with the optical feedback frequency-locking technique, and the device was used to detect multiple trace gases in power transformer diagnosis.

In this work, we developed a cavity-enhanced Raman spectroscopy apparatus for detecting multicomponent trace gases. The sensitivity and linear response of this apparatus are tested through a quantitative CERS measurement of hydrogen. Raman spectra of air, natural gas, and a reference gas mixture of sulfur hexafluoride were recorded to demonstrate the performance of the CERS instrument, which also presents applications for quantitative analysis of multicomponent samples.

In the next section, we present the introduction of the experimental setup. Tests of the performance of the CERS instrument are given in the third section, which consists of measurements of rotational and vibrational Raman spectroscopy of H_2 and other molecules. The fourth section presents applications of the instrument for ambient air, natural gas, and sulfur hexafluoride reference gas samples. A short conclusion will be given in the last section.

■ EXPERIMENTAL SECTION

The experimental configuration of the CERS setup for multiple trace gases analysis is shown in Figure 1. A 1064 nm narrow-
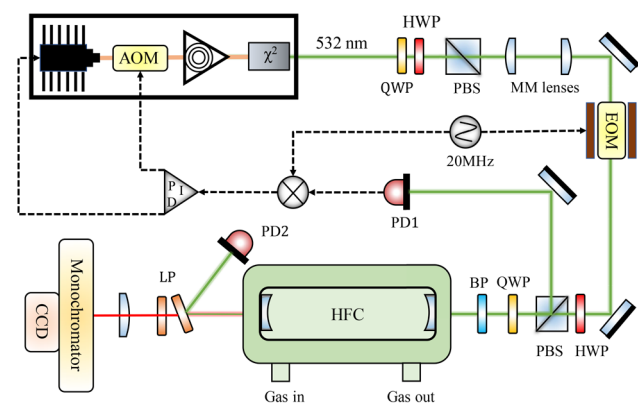

Figure 1. Schematic diagram of the cavity-enhanced Raman spectroscopy setup. OI: optical isolator; MM lenses: mode-matching lenses; EOM: electro-optical modulator; BP: band-pass filter; PD: photodetector; HWP, half-wave plate; PBS, polarizing beam splitter; QWP, quarter-wave plate; HFC: high-finesse cavity; LP: long-pass filter.

line width fiber laser frequency doubled to 532 nm was used as the light source. After passing through a group of lenses, the laser beam is coupled to an optical cavity. The incident laser intensity can be changed by adjusting a wave plate and a polarizing beam-splitting prism before entering the cavity. A linear high-finesse cavity (HFC) placed in a stainless steel vacuum chamber is used here, which consists of two high-reflection (HR) mirrors. The cavity length is 72 cm, corresponding to a free spectral range (FSR) of about 208 MHz.

An electro-optical modulator (EOM) is placed in the incident laser beam for phase modulation (20 MHz), and the laser was locked to a longitudinal mode of the resonant cavity by the Pound-Drever-Hall (PDH) method. The output of

detector PD1 is demodulated to generate the PDH error signal. The slow feedback signal from the proportional-integral-derivative (PID) feedback amplifier is sent to the piezoelectric ceramic actuator (PZT) modulation port of the 1064 nm laser, and the other fast feedback signal is applied to the acousto-optic modulators (AOM) modulation port of the laser.

Emission from the cavity is monitored by the detector PD2, which measured the total intensity of the forward Raman scattering light and the transmitted 532 nm pump light. The input laser power I_{in}, the power inside the cavity I_c, and the power transmitted from the cavity I_{out} have the following relations[24]

$$\frac{I_{out}}{I_c} = t \tag{2}$$

$$\frac{I_{out}}{I_{in}} = \frac{t^2}{(t + l + \alpha L)^2} \tag{3}$$

where t and l are the transmittance and loss of each HR mirror, α is the coefficient of sample absorption/scattering, and L is the length of the cavity. Note that $r + t + l = 1$. Both HR mirrors used in this work have a curvature radius of 100 cm. Ring-down time of the empty cavity at 532 nm was measured to be about 60 μs, leading to a mirror reflectivity of $r = 99.996\%$ and a cavity finesse of $\mathcal{F} = \frac{\pi}{1-r} = 78\,500$. The transmittance of the empty cavity ($\alpha = 0$) was measured to be about 2.7%. Therefore, we obtained $t = 6.6 \times 10^{-6}$ and $l = 33.4 \times 10^{-6}$ according to eq 3, and the light intensity inside the cavity could be about 4000 times that of the incident light.

Two long-pass filters (BLP01-532R-25) block the pump laser and Rayleigh scattering light below 537 nm. The Raman scattered light was focused by a lens with a focal length of 100 mm into a grating spectrometer (Andor750) and recorded by a charge-coupled device (CCD) camera (DV401A-BVF, 200-1100 nm). In this work, we used a grating of 1200 grooves/mm. The measured width of a Raman peak is 0.03−0.06 nm limited by the resolution of the spectrometer, which is much larger than the Doppler width.

The HFC is the most fragile part of the instrument, in particular, the HR mirrors. The mirrors must be protected from dust, condensation, and corrosive gases. We used filters (FISS-ML6−7) to remove particles from the sample gases. A purging flow near the mirrors could be applied if necessary to protect them from corrosive or condensate samples, similar to the method used in ref 25. Vibration isolation is mandatory to maintain the locking servo. The HFC and surrounding optics were placed on an optical table. Some Teflon tubes were placed between the aluminum HFC and the stainless steel sample gas cell, which can support the HFC and reduce the high-frequency vibrations. We did not find the influence due to the slow temperature drift when we have a 2−3 °C temperature drift in the laboratory. The PDH locking servo could be maintained for many hours. A demonstration of a 1 day-long continuous measurement is presented in the Supporting Information.

The CERS approach increases the sensitivity by generating a high circulating power inside the sample cell. Since the input laser power is usually limited in many applications, it is more attractive to use a cavity with higher finesse. However, when cavity mirrors with higher reflectivity are used, cavity modes become narrower, and, consequently, it is more difficult to match the laser frequency with the cavity. That is one reason
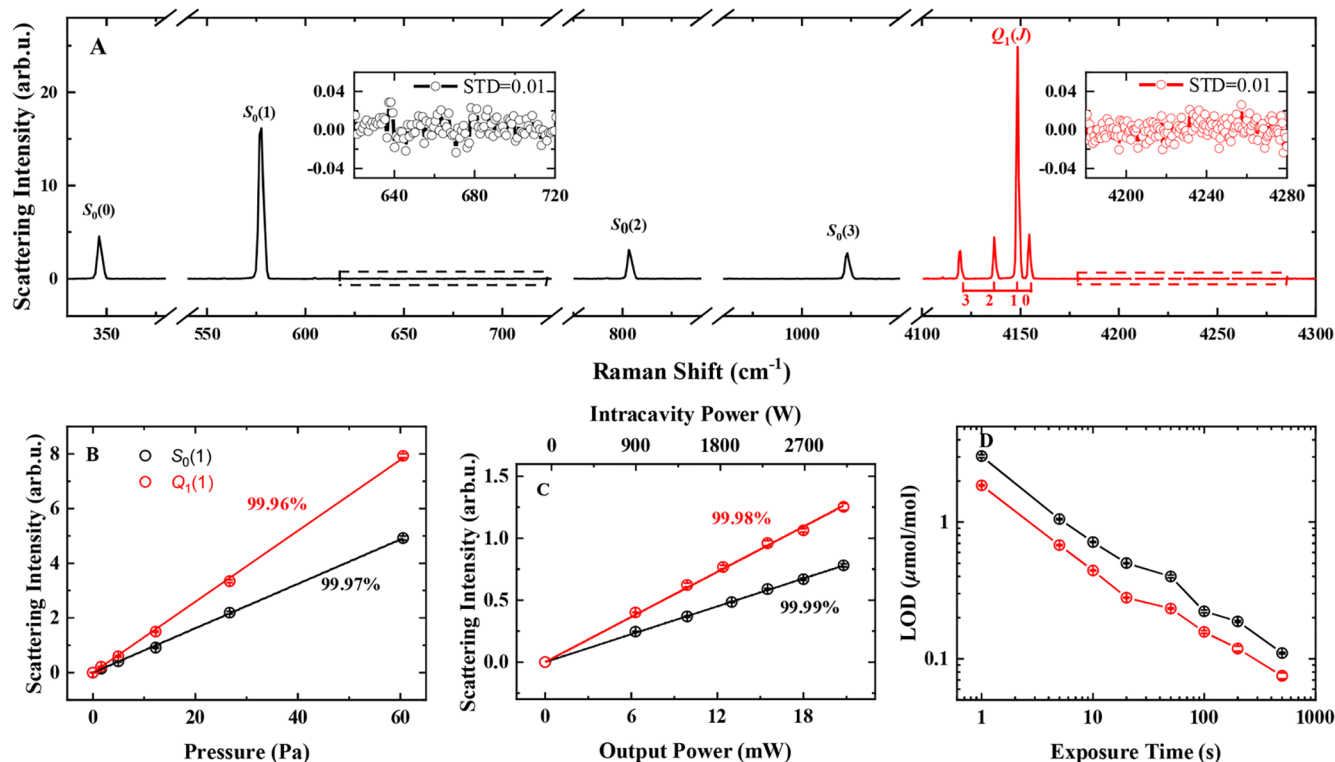
Figure 2. (A) Raman spectrum of the rotational and rovibrational bands of hydrogen, monitoring of the Raman signal at 587 and 4155 cm^{-1} at various pressures and laser powers. (B) Linear dependence of the Raman signal intensity on the hydrogen gas pressure. (C) Peak heights of both rotational and vibrational Raman signals of H_2 increase linearly with the laser power. (D) The LOD was for hydrogen with different exposure times. In (B−D), black circles and red triangles represent the rotational Raman signal $S_0(1)$ at 587 cm^{-1} and the vibrational Raman signal $Q_1(1)$ at 4155 cm^{-1}, respectively.

that most previous CERS measurements[2,22] used cavities with finesses around a few thousand. When a cavity with a finesse of 78 500 is used in this work, an appropriate frequency-locking method is required to keep the input laser frequency locked with the cavity. Wang et al.[23] used the optical feedback frequency-locking (OFFL) method to lock the laser with the cavity with a finesse of 39 200. However, it has been observed[26,27] that the capture range of the OFFL method is often limited and could be sensitive to environmental drifts, which hinders long-term operations. Here we use the PDH locking method to lock a narrow-line-width fiber laser with the cavity. As shown in the result given in the Supporting Information, we can lock the laser very tightly with the cavity, and the locking could be maintained for many hours, which is very useful for real-world applications.

■ PERFORMANCE TEST

Quantitative Measurement of H_2. Real-time and highly sensitive detection of hydrogen is required in various applications, such as nuclear industry safety monitoring, electrical equipment malfunction evaluation, and battery characterization.[28,29] The hydrogen molecule has no electric dipole transitions in the infrared but relatively strong vibrational and rotational Raman transitions. We recorded the Raman spectroscopy of hydrogen to test the system for quantitative measurements, and the results are shown in Figure 2.

In the measurement, we filled the cavity with a mixture of hydrogen and helium with a total pressure of 100 kPa and recorded the Raman spectra at room temperature. Figure 2A

shows typical Raman spectra of 100 ppm of H_2/He with an exposure time of 200 s, including rotational transitions near 587 cm^{-1} (red line) and rovibrational transitions around 4155 cm^{-1} (black line), where $S_0(J)$ (J = 0,1,2,3) denotes the transition $(V = 0, J + 2) \leftarrow (0, J)$, and $Q_1(J)$ is the transition of $(V = 1, J) \leftarrow (0, J)$. Two insets in Figure 2A show the noise levels of the recorded Raman spectra. The intensity of the Raman signal of molecules depends on the intracavity laser power, the gas pressure, and the exposure time. We measured the Raman spectra of H_2 under different partial pressures of hydrogen and different laser powers. Figure 2B shows the measured Raman signal intensities of the $Q_1(1)$ (red) and $S_0(1)$ (black) lines of H_2 when the hydrogen concentration (χ_{H2}) varies in the range of 10−600 μmol/mol. The laser power transmitted from the cavity (I_{out}) was 21.4 mW, and the exposure time (T_{exp}) was 10 s. The results show an excellent linear relationship between the Raman scattering intensity (peak height) and the partial pressure of the hydrogen. Figure 2C shows the scattering intensities of the Raman signal measured under different laser powers. For instance, when the hydrogen concentration was 100 ppm and the exposure time was 10 s, an excellent linear relationship existed between the signal intensity and the laser power transmitted from the cavity. The laser power inside the cavity could be estimated[24] as the laser power transmitted from the cavity multiplied by a factor of 150 000.

According to the height of the Raman signal of H_2 and the noise level, we can estimate the limit of detection (LOD) for hydrogen. As shown in Figure 2A, under the experimental conditions (I_{out} = 21 mW, T_{exp} = 200 s, and χ_{H2} = 100 μmol/
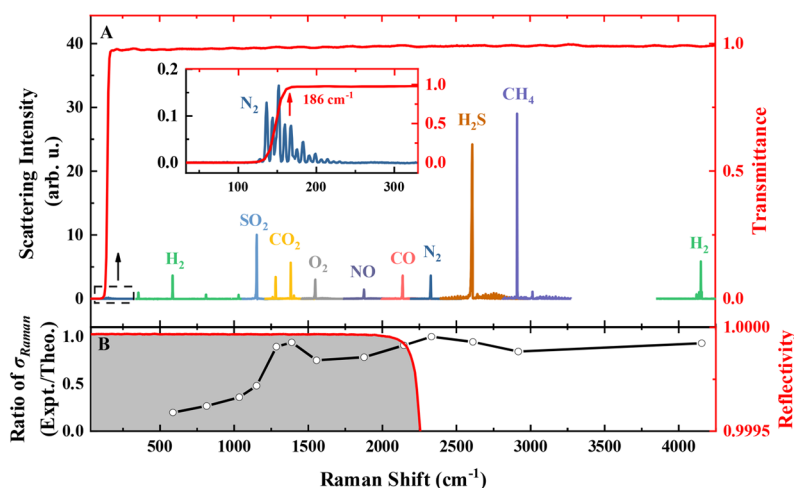
Figure 3. (A) Raman spectra of various molecules. The intensities of all Raman lines were normalized by the exposure time, the intracavity laser power, and the gas pressure. The red curve shows the transmittance of the long-pass optical filter placed before the grating spectrometer, which blocks light below 537 nm (Raman shift <186 cm^{-1}). (inset) The observed rotational Raman lines of N_2 near the cutting edge of the filter. (B) Ratio between the experimental Raman scattering cross-section and the theoretical value (listed in Table 1). The shadow region indicates the stated high-reflectance range of the cavity mirrors.

mol), the Raman signal heights for $S_0(1)$ and $Q_1(1)$ are 16 and 25, respectively. Taking the noise level of 0.01 as the standard deviation (STD) shown in the insets of Figure 2A, we can give LODs for hydrogen using the $S_0(1)$ and $Q_1(1)$ signals that are 0.19 and 0.12 μmol/mol, respectively. The LOD value also changes with the exposure time, and the results are shown in Figure 2D. A longer exposure time improves the detection sensitivity, and LOD roughly changes linearly with $(T_{exp})^{-1/2}$. When the exposure time increases to more than 500 s, the detection limit of the system for hydrogen can be better than 0.1 μmol/mol. In addition, increasing the intracavity laser power could also reduce LOD.

Other Molecules and the Cavity Effect. The intensity of the Raman scattering signal should be proportional to the Raman scattering cross-section of the molecule under the same experimental conditions (gas partial pressure, laser power, and exposure time). Using the 532 nm laser as the excitation light source, the $S_0(1)$ and $Q_1(1)$ Raman transitions of H_2 are located at 549.14 and 682.96 nm. The relative Raman scattering ratios for these two peaks according to the calculated results against the Raman cross-section of nitrogen from literature[30,31] are 4.66 and 1.60; however, our measured data give ratios of 0.92 and 1.49. Since HR mirrors used in this work have a reflectivity of 99.996% in the range of 490−605 nm, the optical resonator also affects the $S_0(1)$ forward Raman scattering signal in this range. While the $Q_1(1)$ signal locates outside the high-reflective region, there is no such effect.

In order to quantitatively evaluate the effect of the resonant cavity on the Raman scattered light, we measured Raman scattering spectra of various molecules, where part of the Raman peaks are covered by the resonant cavity and others are outside. The measured results are shown in Figure 3A. Different colored lines represent different molecules, including H_2, SO_2, CO_2, O_2, NO, CO, N_2, H_2S, and CH_4. Raman spectra plotted in Figure 3A have been normalized to the intracavity laser power, sample gas pressure, and exposure time. The overview of Raman shifts, corresponding transitions, and the relative Raman scattering cross sections is summarized in Table 1. To be noticed here, we further divide the normalized

Table 1. Overview of Raman Shifts, Transitions, Relative Raman Scattering Cross Sections Normalized to the Cross-Section of Nitrogen, and Achieved Limits of Detection for Multiple Gases with an Exposure Time of 500 s

Molecule	Raman shift cm^{-1}	Transition	Relative Raman scattering cross-section Theo.	Relative Raman scattering cross-section Expt.	LOD[a] μmol/mol	Ref
H_2	587	$S_0(1)$	4.66	0.92	0.120	30,31
	815	$S_0(2)$	0.65	0.17		
	1036	$S_0(3)$	0.42	0.16		
SO_2	1151	ν_1	5.20	2.49	0.045	30
CO_2	1285	ν_-	0.95	0.85	0.131	31
	1388	ν_+	1.50	1.41	0.079	
O_2	1556	Q-branch	1.00	0.75	0.148	31
NO	1877	ν_1	0.46	0.36	0.308	31
CO	2145	Q-branch	1.00	0.91	0.122	31
N_2	2331	Q-branch	1.00	1.00	0.111	31
H_2S	2611	ν_1	6.40	6.05	0.018	31
CH_4	2917	ν_1	8.60	7.25	0.015	31
H_2	4155	$Q_1(1)$	1.60	1.49	0.069	30,31

[a]LOD, the limit of detection, defined as the minimum partial pressure of the target molecule, when the amplitude of the Raman scattering signal is three times the noise level.

Raman signal intensity of each molecule by the signal of N_2 for the convenience of discussion, and the results are shown in the fifth column of Table 1. Their corresponding Raman scattering cross-section ratios given in the literature are also listed in this Table. Ratios between experimental and literature values are displayed in Figure 3B as well. The experimental intensities of the Raman signal for different molecules agree well with the literature values when the Raman shifts are greater than 2264 cm^{-1} since the mirror reflectivity is lower than 99.95% (cavity finesse smaller than 6300) in the region above 2264 cm^{-1}. For the Raman shifts less than 2264 cm^{-1}, a relative deviation up to 80% could be observed, since the high-finesse optical cavity could also significantly affect the forward Raman signal.
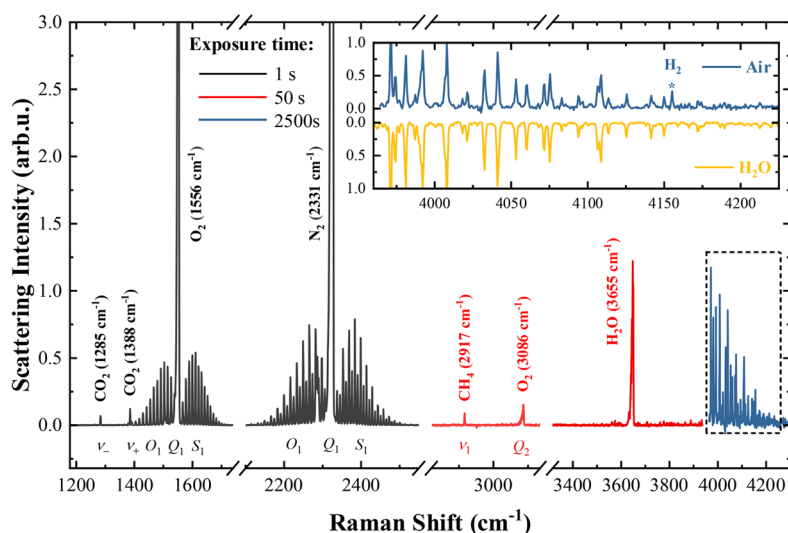
Figure 4. CERS of an ambient air sample (P_{tot} = 100 kPa, I_{in} = 110 mW, and I_{out} = 3 mW). Spectra with the exposure time of 1, 50, and 2500 s are presented in black, red, and dark blue lines, respectively. The inset plot shows the spectrum of ambient air (dark blue line) in the range of 3960–4225 cm^{-1} recorded under an exposure time of 2500 s. Except for the H_2 line at 4155 cm^{-1}, other lines are all assigned to H_2O by comparison to the Raman spectrum of pure water (dark yellow line).

There are numerous Raman rotational transitions of N_2 achieved around 186 cm^{-1} as seen in the zoomed-in plot of Figure 3A, which is consistent with the red curve indicating the transmittance of the optical filter before the grating spectrometer. Based on the measurement capabilities of our system, we expect the limited spectral transmission range to be as low as 186 cm^{-1}. According to the experimentally measured Raman signal intensity of each molecule, similar to the LOD for H_2, we derive the LOD for each molecule as well, and the results are listed in Table 1. For convenience, the values are normalized with the conditions I_{out} = 21 mW, T_{exp} = 10 s, and partial gas pressure P_{tot} = 0.04 kPa. Using our present instrument, we can increase the inlet laser power to 1.2 W, which corresponds to a transmitted laser power of I_{out} = 20 mW, and LODs for most molecules are well below 0.3 μmol/mol with an exposure time of 500 s.

The sensitivity could be further improved by increasing the circulating laser power inside the cavity. However, there are several limitations to that. First, the damage threshold of the HR mirrors used in this work is stated to be over 20 MW/cm^2. We estimated that the laser power density on the mirror surfaces is about 0.8 MW/cm^2 when we used an input laser power of 1.2 W. Although there may be still room to increase the power, we did not try for safety. Second, the HR mirror has a loss of about 6 ppm, and eventually, it may result in heating the mirror. With the presence of the high-power laser, the heating effect may lead to displacements and degradation in the reflectivity of the mirror. Under an input laser power of 1.2 W, we did not observe a considerable decrease in the reflectivity of the mirrors in this work. The sensitivity of this CERS instrument is almost comparable to other advanced methods with ppbv or even sub-ppbv sensitivities in trace-gas detection, such as gas chromatography–mass spectrometry,[32,33] electrochemical sensor,[34,35] photoacoustic spectroscopy,[36,37] and cavity-enhanced absorption spectroscopy.[38,39] Compared to these methods, the CERS instrument could simultaneously detect multiple gases without pretreatment of the sample gas, allowing for wide applications in many vital fields. In the following section, we measured ambient air,

natural gas, and SF_6 reference gas samples as a demonstration of their real-world applications.

■ APPLICATIONS

Most quantitative measurements need to determine concentrations of multiple gas compositions in the sample. As we have shown in the previous section, the CERS signal has good linearity with the gas pressure, intracavity laser power, and exposure time. Before or after measuring a given sample with our CERS instrument, we measure standard gas samples with known concentrations to calibrate the system, and the concentration of a composition in the sample could be derived by comparing the Raman signal with that of the standard sample after normalizing the signals to unit sample pressure, intracavity laser power, and exposure time. The above procedure could be repeated several times to reduce the influence due to the drift of laser power, detector efficiency, etc.

Ambient Air. As a demonstration, we measured the Raman spectrum of ambient air with the CERS instrument, and the recorded spectrum is displayed in Figure 4. The pressure of the air sample was 100 kPa. The spectrum in the range of 1200–2500 cm^{-1} (black curve seen in Figure 4) is the result obtained with an exposure time of 1 s, showing Raman signals of the main components in the air: N_2, O_2, and CO_2. The peak with a Raman shift of 2331 cm^{-1} corresponds to the Q_1 transition of N_2 (also seen in Table 1), surrounded by multiple vibration–rotation Raman transitions (O_1 and S_1-branches). Vibration–rotation Raman lines of O_2 (O_1 and S_1-branches) appear around the strong Q_1 line at 1556 cm^{-1}. The $\nu_1/2\nu_2$ Fermi resonance pair lines of CO_2 are observed at 1285 cm^{-1} (ν_-) and 1388 cm^{-1} (ν_+). The red curve in Figure 4 is the spectrum measured with an exposure time of 50 s, which shows some other components in air: CH_4 and H_2O. The Raman line at 2917 cm^{-1} corresponds to the ν_1 transition of CH_4 (see Table 1). The peak at 3655 cm^{-1} is attributed to H_2O, surrounded by a series of vibration–rotation Raman lines in the same vibrational band in the range of 3550–3900 cm^{-1}.[40] The peak at 3086 cm^{-1} is the Q_2 (V = 2−0, ΔJ = 0) transition of

the oxygen molecule. With an exposure time of 2500 s, we can identify the $Q_1(1)$ line of H_2 at 4155 cm^{-1}, surrounded by various rotation-vibration lines of H_2O, as shown in the inset of Figure 4. The concentrations of gas components in ambient air are summarized in Table 1, according to the intensities of Raman peaks in the observed spectra. Pure gases of carbon dioxide, nitrogen, oxygen, methane, and water at a pressure of 500 Pa were chosen as the standard gases for quantitative analysis. The relative scattering peak intensity between standard gas and sample gas can be obtained after background correction and normalization of the sample pressure, intra-cavity laser power, and exposure time, which yields the actual concentrations of gas components in ambient air, as summarized in Table 2. As expected, the theoretical values

Table 2. Concentrations of Molecules in the Sample Determined by CERS Measurements

Sample	Molecule	Transition cm^{-1}	Peak height arb.u.	Concentration[a] μmol/mol
Air	CO_2	1285	0.35	806(41)
		1388	0.58	828(44)
	O_2	1556	14.45	213 000(11 000)
	N_2	2331	69.97	776 000(39 000)
	CH_4	2917	0.45	2.8(0.1)
	H_2O	3655	1.23	277(14)
Natural gas	H_2	587	22.74	46(2)
	n-C_5H_{12}	763		<0.5[b]
	iso-C_4H_{10}	795	3.4	0.9(0.7)[b]
	n-C_4H_{10}/iso-C_5H_{12}	831	1.6	0.8(0.6)[b]
	C_3H_8	867	21.78	8(1)
	C_2H_6	993	34.68	220(11)
	CO_2	1388	56.60	10 200(510)
	N_2	2331	103.07	13 600(680)
SF_6	C_2F_6	807	0.14[c]	[50.39]
	CF_4	909	0.10	29(23)[b] [49.65]
	SO_2	1151	0.43	52(41)[b] [98.43]
	CO_2	1388	0.22	47(3) [50.41]
	O_2	1556	0.17	69(55)[b] [98.13]
	CO	2145	0.19	50(2) [51.75]
	N_2	2331	0.71	112(5) [101.66]
	CH_4	2917	0.49	9(1) [9.97]
	H_2	4155	0.11	11(1) [10.02]

[a]Values in parentheses are the standard deviations. Results in brackets are stated concentrations in the reference gas sample with a fractional uncertainty of 2%. [b]Estimated value according to the Raman cross-section value obtained from different measurements. [c]Not available due to the absence of reference Raman cross-section value for C_2F_6.

of oxygen and nitrogen were 21% and 78%, respectively, and the deviation of the experimental values from the theoretical values was within 5%.

Natural Gas. Natural gas is a rich and environmentally friendly energy source that is widely used in thermal power generation and the chemical industry.[41] The concentration of methane in natural gases usually amounts to more than 80%, mixed with other heavier hydrocarbons, C_2H_6, C_3H_8, C_4H_{10}, C_5H_{12}, etc., and marginally some other molecules, such as H_2S, He, and N_2.[42] Natural gases from different sources are transported and distributed in modern transmission networks.[43] However, the chemical composition of natural gases

varies substantially in different deposits.[44] A high-sensitivity and multicomponent analysis of natural gases is often required in the transportation and refining of natural gas, which is necessary for balancing the networks as well as in production, trade, and other applications.[45] In this regard, Raman spectroscopy has become a promising method for measuring such gas mixtures.[46]

A natural gas sample was taken from one of the natural gas mines in China. The Raman spectra of the sample are presented in Figure 5 with the sample pressure of 64 kPa. Raman peaks of methane cover a wide range as shown in the figure. The spectrum around 3000 cm^{-1} includes five interacting bands (pentad), the CH stretching bands ν_1 and ν_3, the bending overtones $2\nu_2$ and $2\nu_4$, and the combination band $\nu_2 + \nu_4$, spreading in the range between 2200 and 3400 cm^{-1}. The fundamental bending dyad has two bands, ν_2 and ν_4, spreading in the region of 1200−2000 cm^{-1}.

Characteristic Raman peaks of other alkanes higher than 1000 cm^{-1} are almost covered by the spectrum of CH_4. The black curve in Figure 5 is the Raman spectrum obtained at an exposure time of 100 s. The saturated parts on the middle and right sides are characteristic Raman peaks of the principal component CH_4. The N_2 peak located at 2331 cm^{-1} and the CO_2 lines at 1285 and 1388 cm^{-1} were also observed. There are no O_2 lines observed in the spectrum, indicating that the sample was not contaminated by air.

In the lower-frequency region, Raman peaks of alkanes are mostly attributed to C−C stretching modes, which exclude the interference of CH_4. Assignments of the Raman spectra of hydrocarbons, such as C_2H_6, C_3H_8, and C_nH_{2n+2} ($n \geq 4$), were carried out according to Raman studies on C2−C6 alkanes in the literature.[47−50] The peak with a Raman shift of 993 cm^{-1} corresponds to the C−C stretching band of C_2H_6, as displayed in the zoomed-in plot of Figure 5. The red curve presents the spectrum measured with an exposure time of 2500 s, which indicates that this natural gas sample contains other trace components: H_2, C_3H_8, and alkanes with longer carbon chains. $S_0(1)$ and $S_0(2)$ rotational Raman transitions of H_2 were observed at 587 and 815 cm^{-1}. The 867 cm^{-1} line corresponds to the C−C stretching band of C_3H_8. The 795 cm^{-1} line is attributed to the C−C stretching band of iso-C_4H_{10}. The 831 cm^{-1} line is the characteristic peak that corresponds to the mutual overlaps of n-C_4H_{10} and iso-C_5H_{12}. We did not observe the characteristic peak of n-C_5H_{12} at 763 cm^{-1}, and therefore the content of n-C_5H_{12} in this natural gas sample is estimated to be below 0.5 μmol/mol.

Concentrations of different molecules in the natural gas sample are then determined through the intensities of the Raman peaks, and the results are given in Table 2. The pure gas samples of H_2, CO_2, N_2, C_2H_6, and C_3H_8 were used to calibrate the concentrations of their corresponding species through the normalized Raman signals. The reported Raman intensities of C_nH_{2n+2} ($n \geq 4$) related to C_3H_8 from Petrov et al.[50] were used to estimate concentrations of C4−C5 alkanes.

SF$_6$ Reference Gas for GIS Diagnosis. Sulfur hexafluoride is widely used in gas-insulated switchgear (GIS) in power equipment.[51] It suffers inevitable defects and induces partial discharge or thermal stress over time.[52] As a result, sulfur hexafluoride decomposes and produces various toxic and corrosive byproducts, including SO_2, CF_4, SO_2F_2, SOF_2, SOF_4, HF, H_2S, etc., which in turn affect its overall insulation properties.[53] By monitoring the concentrations of these decomposition contents in GIS, one can provide an on-site
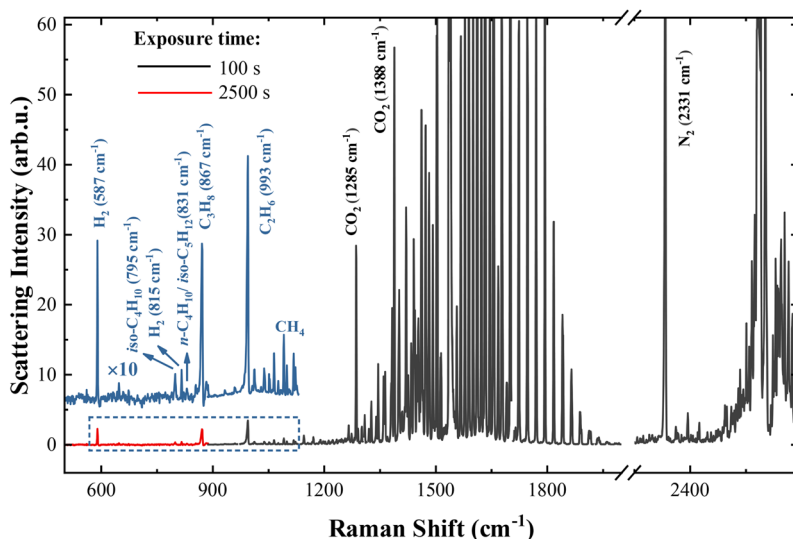
Figure 5. CERS of a natural gas sample (P_{tot} = 64 kPa, I_{in} = 100 mW, and I_{out} = 3 mW). Spectra with the exposure time of 100 and 2500 s are presented in black and red lines, respectively. The blue lines of the zoomed-in plots show the observed H_2 and C2−C5 alkanes.
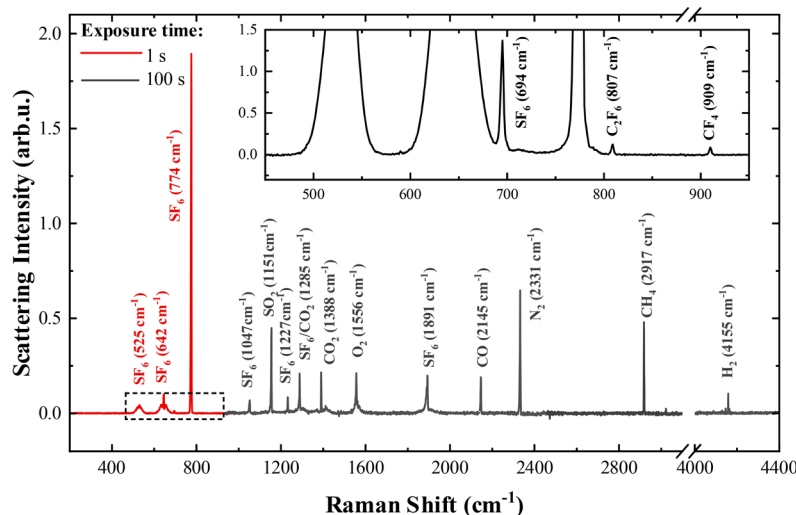

Figure 6. CERS of SF_6 reference spectra (P_{tot} = 50 kPa, I_{in} = 100 mW, I_{out} = 3 mW) with an exposure time of 1 s/100 s are shown in red and black lines. The inset zooms the 694 cm^{-1} peak of SF_6 out, and CF_4, and C_2F_6 peaks well-separated from SF_6 were observed.

diagnosis for power equipment, classify insulation defects, and prevent corrosive decomposition gases from harming the insulation.[54]

In this work, we use the CERS device to measure a reference gas for GIS diagnosis, which is mainly sulfur hexafluoride mixed with some characteristic decomposition gases (H_2, N_2, CO_2, C_2F_6, CF_4, O_2, CO, CH_4, and SO_2). The sample gas is commercially available from Dalian Special Gases Company, and concentrations of these trace gas components are calibrated by gas chromatography. The Raman spectra recorded at a sample pressure of 50 kPa are presented in Figure 6, which includes results at two exposure times of 1 and 100 s. Strong Raman peaks of the main composition SF_6 were observed in the low-frequency range, as shown by the red lines in Figure 6. The strongest line at 774 cm^{-1} is the ν_1 band. Peaks at 694, 642, and 525 cm^{-1} are assigned as the $2\nu_6$, ν_2, and ν_5 bands, respectively.[55] In the high-frequency range, shown in the spectrum recorded with an exposure time of 100 s, the $2\nu_5$, $2\nu_4$, $2\nu_2$, and $2\nu_3$ bands of SF_6 are located with

Raman shifts of 1047, 1227, 1285, and 1891 cm^{-1}, respectively.[56] Besides the SF_6 lines given above, we observed transitions of other trace components in the sample. The characteristic line of C_2F_6 is found at 807 cm^{-1} (ν_2), CF_4 is identified from the line at 909 cm^{-1} (ν_1), the line at 1151 cm^{-1} is attributed to SO_2 (ν_1), and the line at 2145 cm^{-1} corresponds to the Q_1 line of CO.[31,57,58] Lines at 1388, 1556, and 2331 cm^{-1} come from CO_2, O_2, and N_2. The CO_2 line at 1285 cm^{-1} is overlapped by a line of SF_6. We also observed the CH_4 line at 2917 cm^{-1} and the H_2 line at 4155 cm^{-1}.

Concentrations of the above components were derived according to the intensities of representative Raman peaks, and the results are given in Table 2. The reference gas sample and pure gas samples of CO_2, CO, N_2, CH_4, and H_2 were measured alternately multiple times, and quantitative analysis was achieved by comparing Raman scattering intensities. The statistical uncertainty of the derived concentrations is around 5%, and the deviation between the stated concentrations of gas

components from the reference gas is around 10%. Taking into account the influence of the cavity mirrors, as discussed in the previous section, we chose CO_2 as a reference for O_2 and SO_2. The Raman scattering cross-section ratio of CO_2 measured before is used to estimate the component concentrations of O_2 and SO_2, which results in a relatively large discrepancy with the stated values in the reference gas samples. Long et al.[59] reported the relative Raman intensity of CF_4 (ν_1, 909 cm^{-1}) related to CH_4 (ν_1, 2917 cm^{-1}). Furthermore, considering the correction of the effect of the high-reflectivity mirror and using CO_2 as the internal standard gas, we gave an estimated content of CF_4. Since the calculated Raman cross-sectional value of C_2F_6 was not available in the literature as far as we know, the estimated concentration for C_2F_6 was not given in Table 2.

CONCLUSION

In conclusion, we present a cavity-enhanced Raman spectrometer capable of simultaneous measurement of multiple components with high selectivity and sensitivity. Using a resonant cavity with finesse of about 80 000, the intracavity laser power was enhanced thousands of times, which significantly improves the limits of detection of most molecules. The Raman spectra of H_2 under different experimental conditions have been measured, which shows an excellent linear dependence on the partial pressure, the intracavity laser power, and the exposure time. The detection limit for H_2 is demonstrated to be 0.069 μmol/mol with an exposure time of 500 s. We have also shown that the detection limits for most molecules reach the sub-ppm level, such as SO_2, CO_2, O_2, NO, CO, N_2, H_2S, and CH_4. We also observed that the broad coating range of the high-reflective mirrors could reduce the forward Raman emission signals within this range and a correction should be included in quantitative analysis. The instrument was applied to measure the Raman spectra of ambient air, natural gas, and SF_6 reference gas samples. Besides principal components in these samples, multiple trace components have been identified, and their concentrations were determined from the spectra. The results demonstrate that the instrument is useful for a real-time and in situ analysis of multiple components simultaneously with a small gas sample.

ASSOCIATED CONTENT

Ⓢ Supporting Information

The Supporting Information is available free of charge at https://pubs.acs.org/doi/10.1021/acs.analchem.2c05432.

CERS measurement of H_2, Raman spectra, plots of input laser power coupled to the cavity, laser power transmitted from the cavity, height of Raman peak, normalized height of Raman peak, Allan deviation of H_{norm} and noise level of Raman spectrum (PDF)

AUTHOR INFORMATION

Corresponding Authors

Shui-ming Hu − *Department of Chemical Physics, University of Science and Technology of China, Hefei 230026, China;* ⓞ orcid.org/0000-0002-1565-8468; Email: smhu@ustc.edu.cn

Yan Tan − *Department of Chemical Physics, University of Science and Technology of China, Hefei 230026, China;* ⓞ orcid.org/0000-0003-3073-3152; Email: tanyan@ustc.edu.cn

Authors

Qing-ying Yang − *Department of Chemical Physics, University of Science and Technology of China, Hefei 230026, China*

Zi-han Qu − *State Grid Hubei Electric Power Research Institute, Wuhan 430071, China;* ⓞ orcid.org/0000-0003-2410-3496

Yu Sun − *Institute of Advanced Science Facilities, Shenzhen 518107, China*

An-wen Liu − *Department of Chemical Physics, University of Science and Technology of China, Hefei 230026, China*

Complete contact information is available at:
https://pubs.acs.org/10.1021/acs.analchem.2c05432

Notes

The authors declare no competing financial interest.

REFERENCES

(1) Hanf, S.; Bögözi, T.; Keiner, R.; Frosch, T.; Popp, J. *Anal. Chem.* **2015**, *87*, 982−988.

(2) Sandfort, V.; Goldschmidt, J.; Wöllenstein, J.; Palzer, S. *Sensors* **2018**, *18*, 709.

(3) Sieburg, A.; Schneider, S.; Yan, D.; Popp, J.; Frosch, T. *Analyst* **2018**, *143*, 1358−1366.

(4) Sieburg, A.; Jochum, T.; Trumbore, S. E.; Popp, J.; Frosch, T. *Analyst* **2017**, *142*, 3360−3369.

(5) Barik, P.; Pradhan, M. *Analyst* **2022**, *147*, 1024−1054.

(6) Wang, H.; Chen, J.; Lu, K. *Atmos. Meas. Technol.* **2017**, *10*, 1465−1479.

(7) Maithani, S.; Panda, B.; Maity, A.; Pradhan, M. *J. Phys. Chem. A* **2020**, *124*, 1104−1111.

(8) Wang, C.; Sahay, P. *Sensors* **2009**, *9*, 8230−8262.

(9) Xia, J.; Feng, C.; Zhu, F.; Ye, S.; Zhang, S.; Kolomenskii, A.; Wang, Q.; Dong, J.; Wang, Z.; Jin, W.; Schuessler, H. A. *Sens. Actuat. B Chem.* **2021**, *334*, 129641.

(10) Fathy, A.; Sabry, Y. M.; Hunter, I. W.; Khalil, D.; Bourouina, T. *Laser Photonics Rev.* **2022**, *16*, 2100556.

(11) Banik, G. D.; Mizaikoff, B. *J. Breath Res.* **2020**, *14*, 043001.

(12) McCartt, A. D.; Jiang, J. *ACS Sens* **2022**, *7*, 3258−3264.

(13) Niklas, C.; Wackerbarth, H.; Ctistis, G. *Sensors* **2021**, *21*, 1698.

(14) Jochum, T.; von Fischer, J. C.; Trumbore, S.; Popp, J.; Frosch, T. *Anal. Chem.* **2015**, *87*, 11137−11142.

(15) Spencer, C. L.; Watson, V.; Hippler, M. *Analyst* **2012**, *137*, 1384−1388.

(16) Hanf, S.; Keiner, R.; Yan, D.; Popp, J.; Frosch, T. *Anal. Chem.* **2014**, *86*, 5278−5285.

(17) Salter, R.; Chu, J.; Hippler, M. *Analyst* **2012**, *137*, 4669−4676.

(18) Wang, J.; Chen, W.; Wang, P.; Zhang, Z.; Wan, F.; Zhou, F.; Song, R.; Wang, Y.; Gao, S. *Opt. Express* **2021**, *29*, 32296.

(19) Li, X.; Xia, Y.; Zhan, L.; Huang, J. *Opt. Lett.* **2008**, *33*, 2143−2145.

(20) Smith, T. W.; Hippler, M. *Anal. Chem.* **2017**, *89*, 2147−2154.

(21) Wang, P.; Chen, W.; Wan, F.; Wang, J.; Hu, J. *Opt. Express* **2019**, *27*, 33312.

(22) Taylor, D. J.; Glugla, M.; Penzhorn, R. D. *Rev. Sci. Instrum.* **2001**, *72*, 1970−1976.

(23) Wang, P.; Chen, W.; Wang, J.; Tang, J.; Shi, Y.; Wan, F. *Anal. Chem.* **2020**, *92*, 5969−5977.

(24) Ma, L.-S.; Ye, J.; Dubé, P.; Hall, J. L. *J. Opt. Soc. Am. B* **1999**, *16*, 2255−2268.

(25) Hu, S.; Zhang, F.; Shang, Q.; Chen, J.; Lu, L.; Miao, X.; Niu, L.; Liu, H.; Zhou, G.; Yuan, X. *Optik* **2021**, *231*, 166365.

(26) Ohshima, S. I.; Schnatz, H. *J. Appl. Phys.* **1992**, *71*, 3114−3117.

(27) Manfred, K. M.; Ciaffoni, L.; Ritchie, G. A. *Appl. Phys. B: Laser Opt.* **2015**, *120*, 329−339.

(28) Vafaie, R. H.; Shafiei-pour, R.; Nojavan, S.; Jermsittiparsert, K. *Int. J. Hydro. Energy* **2020**, *45*, 21148−21156.

(29) Hübert, T.; Boon-Brett, L.; Black, G.; Banach, U. *Sens. Actuat. B Chem.* **2011**, *157*, 329−352.

(30) Flora, F.; Giudicotti, L. *Appl. Opt.* **1987**, *26*, 4001−4008.

(31) Fenner, W. R.; Hyatt, H. A.; Kellam, J. M.; Porto, S. P. S. *J. Opt. Soc. Am.* **1973**, *63*, 73−77.

(32) Oliveira, L. F. d.; Mallafre-Muro, C.; Giner, J.; Perea, L.; Sibila, O.; Pardo, A.; Marco, S. *Clin. Chim. Acta* **2022**, *526*, 6−13.

(33) Lu, J.; Li, Y.; Li, J.; Jing, S.; An, T.; Luo, H.; Ma, C.; Wang, H.; Fu, Q.; Huang, C. *J. Chromatogr. A* **2022**, *1677*, 463299.

(34) Li, J.; Zhu, C.; Peng, W.; Cao, X.; Gao, H.; Jiang, M.; Wu, Z.; Yu, C. *Anal. Chem.* **2023**, *95*, 2406−2412.

(35) Kim, S. H.; Yun, K. S. *Sens. Actuat. B Chem.* **2023**, *376*, 132958.

(36) Pangerl, J.; Müller, M.; Rück, T.; Weigl, S.; Bierl, R. *Sens. Actuat. B Chem.* **2022**, *352*, 130962.

(37) Sampaolo, A.; Patimisco, P.; Giglio, M.; Zifarelli, A.; Wu, H.; Dong, L.; Spagnolo, V. *Anal. Chim. Acta* **2022**, *1202*, 338894.

(38) Liang, Q.; Chan, Y.-C.; Changala, P. B.; Nesbitt, D. J.; Ye, J.; Toscano, J. *Proc. Natl. Acad. Sci. U.S.A.* **2021**, *118*, 1−6.

(39) Zhou, J.; Zhao, W.; Zhang, Y.; Fang, B.; Cheng, F.; Xu, X.; Ni, S.; Zhang, W.; Ye, C.; Chen, W.; Venables, D. S. *Anal. Chem.* **2022**, *94*, 3368−3375.

(40) Avila, G.; Fernández, J. M.; Tejeda, G.; Montero, S. *J. Mol. Spectrosc.* **2004**, *228*, 38−65.

(41) Deng, Y.; Dewil, R.; Appels, L.; Van Tulden, F.; Li, S.; Yang, M.; Baeyens, J. *Fuel* **2022**, *318*, 123680.

(42) Scholes, C. A.; Stevens, G. W.; Kentish, S. E. *Fuel* **2012**, *96*, 15−28.

(43) Filimonova, I. V.; Komarova, A. V.; Sharma, R.; Novikov, A. Y. *Energy Rep* **2022**, *8*, 675−682.

(44) Buldakov, M. A.; Korolev, B. V.; Matrosov, I. I.; Petrov, D. V.; Tikhomirov, A. A. *J. Appl. Spectrosc.* **2013**, *80*, 124−128.

(45) Ficco, G.; Dell'Isola, M.; Vigo, P.; Celenza, L. *Flow Meas. Instrum.* **2015**, *42*, 58−68.

(46) Petrov, D. V.; Matrosov, I. I.; Zaripov, A. R.; Tanichev, A. S. *Sensors* **2022**, *22*, 3492.

(47) Magnotti, G.; KC, U.; Varghese, P. L.; Barlow, R. S. *J. Quant. Spectrosc. Radiat. Transfer* **2015**, *163*, 80−101.

(48) Petrov, D. V.; Matrosov, I. I.; Zaripov, A. R. *Opt. Spectrosc.* **2018**, *125*, 5−9.

(49) Knebl, A.; Domes, C.; Domes, R.; Wolf, S.; Popp, J.; Frosch, T. *Anal. Chem.* **2021**, *93*, 10546−10552.

(50) Petrov, D. *Anal. Chem.* **2021**, *93*, 16282−16284.

(51) Li, S.; Li, J. *High Voltage* **2017**, *2*, 82−91.

(52) Zeng, F.; Wu, S.; Lei, Z.; Li, C.; Tang, J.; Yao, Q.; Miao, Y. *IEEE Trans. Dielectr. Electr. Insul.* **2020**, *27*, 581−589.

(53) Zeng, F.; Wu, S.; Yang, X.; Wan, Z.; Tang, J.; Zhang, M.; Yao, Q. *IEEE Access* **2019**, *7*, 29869−29881.

(54) Mahdi, A. S.; Abdul-Malek, Z.; Arshad, R. N. *IEEE Access* **2022**, *10*, 27270−27288.

(55) Shelton, D. P.; Ulivi, L. *J. Chem. Phys.* **1988**, *89*, 149−155.

(56) Kremer, D.; Rachet, F.; Chrysos, M. *J. Chem. Phys.* **2013**, *138*, 174308.

(57) Golubkova, O. S.; Shchepkin, D. N.; Bertsev, V. V.; Sergeev, P. K. *J. Mol. Struct.* **2015**, *1091*, 20−24.

(58) Tabyaoui, A.; Lavorel, B.; Saint-Loup, R.; Rotger, M. *J. Raman Spectrosc.* **1994**, *25*, 255−260.

(59) Long, D. A.; Thomas, E. L. *Trans. Faraday Soc.* **1963**, *59*, 1026−1032.